Combined Path Following and Compliance Control with Application to a Biaxial Gantry Robot

authored by **S. Flixeder, T. Glück, M. Böck, and A. Kugi**

and published in *Proceedings of the IEEE Conference on Control Applications (CCA)*.

Contact:

Automation and Control Institute (ACIN)
Vienna University of Technology
Gusshausstrasse 27-29/E376
1040 Vienna, Austria

Internet: www.acin.tuwien.ac.at
E-mail: office@acin.tuwien.ac.at
Phone: +43 1 58801 37601
Fax: +43 1 58801 37699

Combined Path Following and Compliance Control with Application to a Biaxial Gantry Robot

Stefan Flixeder[1], Tobias Glück[1], Martin Böck[1], and Andreas Kugi[1]

***Abstract*— This work presents an approach to simultaneously, but independently control the compliance of a robotic system transversal and tangential to a given curve. Therefore, a path following control concept known as transverse feedback linearization and a compliance control concept known as admittance control are combined. The subordinate path following controller transforms the nonlinear dynamics into a linear system with decoupled transversal and tangential dynamics via a coordinate and feedback transformation. The outer control loop utilizes admittance control to obtain the desired target compliance in the respective transformed coordinates. The proposed approach is applied to a biaxial gantry robot. Experimental results underline the feasibility of the proposed concept.**

I. INTRODUCTION

The traditional way of planning an automated machining task, such as milling, grinding, deburring or saw cutting, is to define a specific path and a speed parametrization which is subsequently tracked using standard position control. Recent developments in robotized machining processes, see [1] for an overview, make also use of force control [2]. By controlling the material removal rate that depends on the counter force it is possible to react to material inhomogeneities and thus to improve the machining performance. Classical approaches either control the contact force perpendicular to the surface [3] or the feed force — and hence the material removal rate — along the machining path [4]. To the authors knowledge, no attempt has been made so far to independently control both, the force transversal and tangential to the machining path. For this purpose, the authors make use of recent advances in path following control, see, e.g., [5], [6], [7] and well known concepts of compliance control, see, e.g., [8], [9], [10]. By successfully combining these approaches, the proposed control strategy is capable of

- approaching the path from a given starting point,
- controlling the force perpendicular to the path while tracking a given trajectory along the path,
- controlling the force/position perpendicular to the path while manually guiding the position along the path by a human operator,
- controlling the feed force along the path while stabilizing and/or tracking a given trajectory perpendicular to the path and any combination of the previous.

This paper is organized as follows: Section II provides an introduction of the test setup of a two-degree-of-freedom (2-DOF) gantry robot. Moreover, an appropriate mathematical model is developed. Section III briefly summarizes the path following methodology, denoted as transverse feedback linearization, and applies it to the system under consideration. Section IV introduces admittance control, the utilized compliance control concept, and combines it with the transverse feedback linearization. Section V presents experimental results performed on the test setup.

*This work was supported by FESTO AG & CO. KG

[1]The authors are with the Automation and Control Institute (ACIN), Vienna University of Technology, 1040 Vienna, Austria {flixeder;glueck;boeck;kugi}@acin.tuwien.ac.at

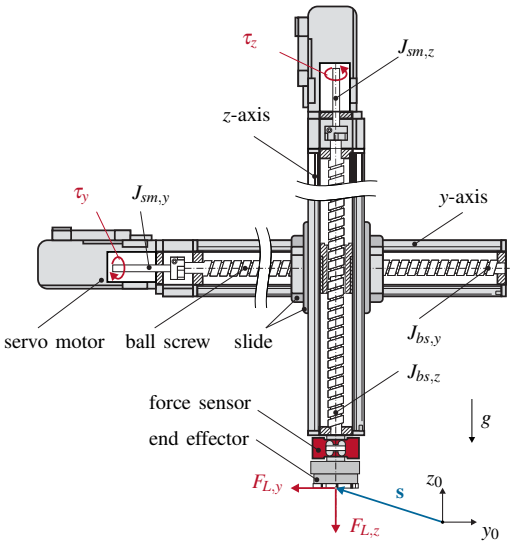

Fig. 1. Schematic diagram of the 2-DOF gantry robot.

II. EXPERIMENTAL SETUP AND MATHEMATICAL MODEL

Consider the schematic diagram of a linear 2-DOF gantry robot depicted in Fig. 1. Each linear drive consists of a servo motor and a ball screw drive. The ball screw drives convert the applied torques into a translational motion of the slides. The coupling between the motor, the ball screw and the slide as well as the mechanic connection of the y- and z-axis is considered stiff and backlash-free. Hence, the dynamics of the two linear axes are decoupled. The servo motors are equipped with fast current controllers allowing to use the actual motor torques τ_i, $i \in \{y,z\}$ as control inputs of the system. In order to measure the external load forces $F_{L,i}$ acting on the end effector, the test setup is equipped with a triaxial force sensor based on strain gauge technology. Let $\mathbf{s}^{\mathrm{T}} = \begin{bmatrix} s_y & s_z \end{bmatrix}$ be the position of the end effector with respect to the reference frame (y_0, z_0), $m_{t,i}$ be the moved translational mass, k_i be the spindle pitch and $m_{J,i} = \left(J_{sm,i} + J_{bs,i}\right)/k_i^2$ be the equivalent mass of the inertia of the servo motor

Post-print version of the article: S. Flixeder, T. Glück, M. Böck, and A. Kugi, "Combined path following and compliance control with application to a biaxial gantry robot", in *Proceedings of the IEEE Conference on Control Applications (CCA)*, Antibes, France, Oct. 2014, pp. 796–801. DOI: 10.1109/CCA.2014.6981438

$J_{sm,i}$ and the ball screw $J_{bs,i}$, respectively. Newtons second law yields the equations of motion $(m_{t,i}+m_{J,i})\ddot{s}_i = F_{M,i} - F_{F,i} - F_{G,i} - F_{L,i}$, where $F_{M,i} = \tau_i/k_i$ is the equivalent motor force, $F_{G,y} = 0$, and $F_{G,z} = g m_{t,z}$ are the gravitational forces, with $g = 9.81\,\mathrm{m\,s^{-2}}$. The precision of the ball screw drives comes at the expense of high internal friction forces, which are approximated by $F_{F,i}(\dot{s}_i) = F_{c,i}\tanh(\dot{s}_i/w) + c_{v,i}\dot{s}_i$, with $w \ll 1$ and the coefficients $c_{v,i} > 0$ and $F_{c,i} > 0$ of the viscous and Coulomb friction, respectively. By introducing the state vector $\mathbf{x}^{\mathrm{T}} = \begin{bmatrix}\mathbf{x}_c^{\mathrm{T}} & \mathbf{x}_v^{\mathrm{T}}\end{bmatrix} \in \mathbb{R}^4$ with $\mathbf{x}_c^{\mathrm{T}} = \begin{bmatrix}s_y & s_z\end{bmatrix}$ and $\mathbf{x}_v^{\mathrm{T}} = \begin{bmatrix}\dot{s}_y & \dot{s}_z\end{bmatrix}$, the input vectors $\mathbf{u}^{\mathrm{T}} = \begin{bmatrix}F_{M,y} & F_{M,z}\end{bmatrix} \in \mathbb{R}^2$ and $\mathbf{d}^{\mathrm{T}} = \begin{bmatrix}F_{L,y} & F_{L,z}\end{bmatrix} \in \mathbb{R}^2$, the equations of motion can be written in the input affine form

$$\dot{\mathbf{x}} = \begin{bmatrix}\mathbf{x}_v \\ \mathbf{f}_v(\mathbf{x}_v)\end{bmatrix} + \begin{bmatrix}\mathbf{0}_{2\times 2} \\ \mathbf{G}_v(\mathbf{x}_c)\end{bmatrix}\mathbf{u} + \begin{bmatrix}\mathbf{0}_{2\times 2} \\ -\mathbf{I}_{2\times 2}\end{bmatrix}\mathbf{d} \tag{1}$$

with

$$\mathbf{f}_v(\mathbf{x}_v) = \begin{bmatrix}\frac{-F_{F,y}(\dot{s}_y)}{m_{t,y}+m_{J,y}} \\ \frac{-F_{F,z}(\dot{s}_z)-g m_{t,z}}{m_{t,z}+m_{J,z}}\end{bmatrix}, \mathbf{G}_v(\mathbf{x}_c) = \begin{bmatrix}\frac{1}{m_{t,y}+m_{J,y}} & 0 \\ 0 & \frac{1}{m_{t,z}+m_{J,z}}\end{bmatrix}. \tag{2}$$

Moreover, the class of outputs $\mathbf{y}$ is restricted to smooth functions of the configuration states $\mathbf{x}_c$ given by

$$\mathbf{y} = \mathbf{h}(\mathbf{x}_c) = \mathbf{x}_c\,, \qquad \mathbf{y} \in \mathbb{R}^2. \tag{3}$$

III. Path Following Control

The objective of the path following problem is to design a smooth feedback control law that makes the system output (3) approach and move along a path γ where no *a priori* time parametrization is associated with the movement on the path. The approach utilized in this paper was introduced as transverse feedback linearization in, e.g., [5] and restricted to the class of mechanical systems in [7]. In the following section, this concept is revisited and applied to the considered 2-DOF gantry robot.

A. Path Assumptions

Suppose the path γ is given as a smooth parametrized curve $\hat{\boldsymbol{\sigma}}(\cdot) : \mathbb{R} \to \mathbb{R}^2$ — not necessarily with a unit speed parametrization[1] $\|\hat{\boldsymbol{\sigma}}'(\cdot)\| = 1$ — and the geometric restrictions on the class of curves imposed in [5] and [11]:

Assumption 1: The parametrization $\hat{\boldsymbol{\sigma}}(\cdot)$ is an embedded submanifold of $\mathbb{R}^2$, which implies that γ has no self-intersections.

Assumption 2: There exists a smooth map $\delta(\cdot) : \mathbb{R}^2 \to \mathbb{R}$ such that the path γ can be represented as the zero-level set of δ in the output space (3) of (1).

Approaching and following the path γ is equivalent to stabilize the submanifold $\Gamma := \{\mathbf{x} \in \mathbb{R}^4 : \delta \circ \mathbf{h}(\mathbf{x}_c) = 0\}$. However, in [5], [7] it is shown that in general Γ is not invariant[2] and thus only the stabilization of the largest controlled invariant subset Γ^* of Γ can be asked for the path following control design. Γ^* can be interpreted as the set of all trajectories for which the output $\mathbf{y}$ according to (3) can be forced to stay on γ for all times by a suitable control input $\mathbf{u}$. It can also be interpreted as the zero-dynamics manifold of (1) with the output $\lambda(\mathbf{x}_c) = \delta \circ \mathbf{h}(\mathbf{x}_c)$. For more details, the reader is kindly referred to [5], [6], [7].

[1] In the following, $\|\cdot\|$ refers to the Euclidean norm and $\hat{\boldsymbol{\sigma}}'(\hat{\theta}) = \frac{\mathrm{d}\hat{\boldsymbol{\sigma}}}{\mathrm{d}\hat{\theta}}$.

[2] A set of states $\Gamma \subseteq \mathbb{R}^4$ of the system (1) is called an invariant set of (1) if for all $\mathbf{x}(0) \in \Gamma$ and for all $t \geq 0$, $\mathbf{x}(t) \in \Gamma$.

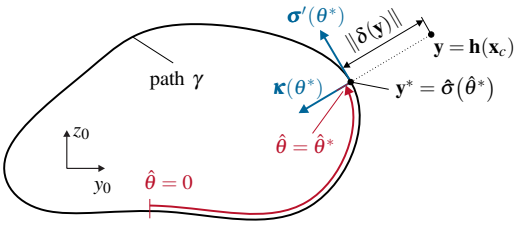

Fig. 2. Path illustration.

B. Transverse and Tangential Feedback Linearization

The fundamental idea of the transverse feedback linearization concept is to find a coordinate transformation $\mathbf{T} : \mathbf{x} \mapsto (\boldsymbol{\eta}, \boldsymbol{\xi})$, defined in a neighborhood of γ, and a feedback transformation such that the system (1) transforms and decomposes into a tangential $\boldsymbol{\eta}$- and a transversal $\boldsymbol{\xi}$-subsystem with respect to γ. Following Theorem 3.2 of [7], the system (1)-(3) is locally transverse feedback linearizable. Subsequently, the derivation of the coordinate transformation $\mathbf{T} : \mathbf{x} \mapsto (\boldsymbol{\eta}, \boldsymbol{\xi})$ for a given curve $\hat{\boldsymbol{\sigma}}(\cdot)$ will be shown in detail.

Therefore, a projection operator $\hat{\boldsymbol{\varpi}}$ that maps each point $\mathbf{y} \in \gamma_\varepsilon$ in a tubular neighborhood γ_ε of the closed curve[3] to a unique parameter $\hat{\theta}^* \in [0, \hat{L})$, with $\hat{\boldsymbol{\sigma}}(\hat{\theta}^* + \hat{L}) = \hat{\boldsymbol{\sigma}}(\hat{\theta}^*)$ is introduced. In order to calculate the point $\mathbf{y}^* = \hat{\boldsymbol{\sigma}}(\hat{\theta}^*)$ on the path γ that is closest to $\mathbf{y}$ in the sense of a given metric, the minimization problem

$$\hat{\theta}^* = \hat{\boldsymbol{\varpi}}(\mathbf{y}) := \arg\min_{\hat{\theta} \in [0, \hat{L})} \left\|\mathbf{y} - \hat{\boldsymbol{\sigma}}(\hat{\theta})\right\| \tag{4}$$

has to be solved [6]. The tangential state $\eta_1 = \pi(\mathbf{x}_c)$ is chosen as $\eta_1 = g \circ \mathbf{h}(\mathbf{x}_c)$ with

$$\theta^* = g(\mathbf{y}) = \left(\int_0^{\hat{\theta}^*} \left\|\hat{\boldsymbol{\sigma}}'(\tau)\right\| \mathrm{d}\tau\right)\Bigg|_{\hat{\theta}^* = \hat{\boldsymbol{\varpi}}(\mathbf{y})}. \tag{5}$$

Clearly, the *tangential unit vector on the path* reads as $\boldsymbol{\sigma}'(\theta^*) = \hat{\boldsymbol{\sigma}}'(\hat{\theta}^*)/\left\|\hat{\boldsymbol{\sigma}}'(\hat{\theta}^*)\right\|$. The *transversal unit vector* $\boldsymbol{\kappa}(\theta^*)$ is obtained by a counter clockwise rotation of $\pi/2$, i.e., $\boldsymbol{\kappa}(\theta^*) = \mathbf{R}_{\pi/2}\boldsymbol{\sigma}'(\theta^*)$ with the associated rotation matrix $\mathbf{R}_{\pi/2}$. See Fig. 2 for a graphic representation. Since $\mathbf{y} - \hat{\boldsymbol{\sigma}}(\hat{\theta}^*)$ is parallel to $\hat{\boldsymbol{\kappa}}(\hat{\theta}^*) = \mathbf{R}_{\pi/2}\hat{\boldsymbol{\sigma}}'(\hat{\theta}^*)/\left\|\hat{\boldsymbol{\sigma}}'(\hat{\theta}^*)\right\|$, the output may be written in the form $\mathbf{y} = \hat{\boldsymbol{\sigma}}(\hat{\theta}^*) + \hat{\boldsymbol{\kappa}}(\hat{\theta}^*)\delta(\mathbf{y})$ and solved for

$$\delta(\mathbf{y}) = \frac{1}{\left\|\hat{\boldsymbol{\sigma}}'(\hat{\theta}^*)\right\|}\left(\mathbf{R}_{\pi/2}\hat{\boldsymbol{\sigma}}'(\hat{\theta}^*)\right)^{\mathrm{T}}\left(\mathbf{y} - \hat{\boldsymbol{\sigma}}(\hat{\theta}^*)\right)\Bigg|_{\hat{\theta}^* = \hat{\boldsymbol{\varpi}}(\mathbf{y})}.$$

The length of $\delta(\mathbf{y})$ is exactly the measure of the distance of the point $\mathbf{y}$ to the corresponding point $\mathbf{y}^* = \boldsymbol{\sigma}(\theta^*)$ on the curve γ. Thus, we choose $\xi_1 = \lambda(\mathbf{x}_c) = \delta \circ \mathbf{h}(\mathbf{x}_c)$ as the first transversal state.

[3] See [11] for non-closed curves.

Post-print version of the article: S. Flixeder, T. Glück, M. Böck, and A. Kugi, "Combined path following and compliance control with application to a biaxial gantry robot", in *Proceedings of the IEEE Conference on Control Applications (CCA)*, Antibes, France, Oct. 2014, pp. 796–801. DOI: 10.1109/CCA.2014.6981438

For the coordinate transformation $\mathbf{T}:\mathbf{x}\mapsto(\boldsymbol{\eta},\boldsymbol{\xi})$ the time derivatives of η_1 and ξ_1 are required. Although in general $\hat{\theta}^*$ from (4) can only be calculated numerically, an analytical expression can be found for its time derivative based on the necessary optimality condition of (4), i.e.,

$$\left(\mathbf{y}-\hat{\boldsymbol{\sigma}}\left(\hat{\theta}^*\right)\right)^{\mathrm{T}}\hat{\boldsymbol{\sigma}}'\left(\hat{\theta}^*\right)=0. \tag{6}$$

Performing the time derivative of (6) yields

$$\left(\dot{\mathbf{y}}-\hat{\boldsymbol{\sigma}}'\left(\hat{\theta}^*\right)\dot{\hat{\theta}}^*\right)^{\mathrm{T}}\hat{\boldsymbol{\sigma}}'\left(\hat{\theta}^*\right)+\left(\mathbf{y}-\hat{\boldsymbol{\sigma}}\left(\hat{\theta}^*\right)\right)^{\mathrm{T}}\hat{\boldsymbol{\sigma}}''\left(\hat{\theta}^*\right)\dot{\hat{\theta}}^*=0$$

and with $\mathbf{y}-\hat{\boldsymbol{\sigma}}\left(\hat{\theta}^*\right)=\mathbf{R}_{\pi/2}\hat{\boldsymbol{\sigma}}'\left(\hat{\theta}^*\right)/\left\|\hat{\boldsymbol{\sigma}}'\left(\hat{\theta}^*\right)\right\|\delta(\mathbf{y})$ we get from (5)

$$\dot{\eta}_1=\left\|\hat{\boldsymbol{\sigma}}'\left(\hat{\theta}^*\right)\right\|\dot{\hat{\theta}}^*=\underbrace{\frac{1}{1-\varphi'\delta(\mathbf{y})}\frac{\left(\hat{\boldsymbol{\sigma}}'\left(\hat{\theta}^*\right)\right)^{\mathrm{T}}}{\left\|\hat{\boldsymbol{\sigma}}'\left(\hat{\theta}^*\right)\right\|}\Big|_{\hat{\theta}^*=\hat{\boldsymbol{\varpi}}(\mathbf{y})}}_{\mathrm{d}\eta_1}\underbrace{\dot{\mathbf{y}}}_{\mathrm{d}\mathbf{h}\ \mathbf{x}_v}$$

with $\dot{\eta}_1=\eta_2$ and

$$\varphi'=\frac{\left(\mathbf{R}_{\pi/2}\hat{\boldsymbol{\sigma}}'\left(\hat{\theta}^*\right)\right)^{\mathrm{T}}\hat{\boldsymbol{\sigma}}''\left(\hat{\theta}^*\right)}{\left\|\hat{\boldsymbol{\sigma}}'\left(\hat{\theta}^*\right)\right\|^3}\Big|_{\hat{\theta}^*=\hat{\boldsymbol{\varpi}}(\mathbf{y})},\quad \mathrm{d}\mathbf{h}=\frac{\partial\mathbf{h}(\mathbf{x}_c)}{\partial\mathbf{x}_c}.$$

Analogously, it can be shown that the time derivative of ξ_1 reads as

$$\dot{\xi}_1=\xi_2=\underbrace{\frac{\left(\mathbf{R}_{\pi/2}\hat{\boldsymbol{\sigma}}'\left(\hat{\theta}^*\right)\right)^{\mathrm{T}}}{\left\|\hat{\boldsymbol{\sigma}}'\left(\hat{\theta}^*\right)\right\|}\Big|_{\hat{\theta}^*=\hat{\boldsymbol{\varpi}}(\mathbf{y})}}_{\mathrm{d}\xi_1}\underbrace{\dot{\mathbf{y}}}_{\mathrm{d}\mathbf{h}\ \mathbf{x}_v}.$$

Thus, the coordinate transformation $\mathbf{T}$ takes the form

$$\begin{bmatrix}\eta_1\\ \eta_2\\ \xi_1\\ \xi_2\end{bmatrix}=\begin{bmatrix}\pi(\mathbf{x}_c)\\ \mathrm{d}\pi\mathbf{x}_v\\ \lambda(\mathbf{x}_c)\\ \mathrm{d}\lambda\mathbf{x}_v\end{bmatrix}=\begin{bmatrix}g\circ\mathbf{h}(\mathbf{x}_c)\\ \mathrm{d}\eta_1\mathrm{d}\mathbf{h}\ \mathbf{x}_v\\ \delta\circ\mathbf{h}(\mathbf{x}_c)\\ \mathrm{d}\xi_1\mathrm{d}\mathbf{h}\ \mathbf{x}_v\end{bmatrix}, \tag{7}$$

where $\mathrm{d}\lambda=\partial\lambda(\mathbf{x}_c)/\partial\mathbf{x}_c$ and $\mathrm{d}\pi=\partial\pi(\mathbf{x}_c)/\partial\mathbf{x}_c$. These results are also in accordance with [6]. Note that $\mathrm{d}\lambda$ and $\mathrm{d}\pi$, are given analytically and $\|\mathrm{d}\eta_1\|=\|\mathrm{d}\xi_1\|=1$ holds for any point $\mathbf{y}^*$ on the curve.

Along the lines of [7],

$$\tilde{\mathbf{y}}=\begin{bmatrix}\lambda(\mathbf{x}_c)\\ \pi(\mathbf{x}_c)\end{bmatrix}=\begin{bmatrix}\delta\circ\mathbf{h}(\mathbf{x}_c)\\ g\circ\mathbf{h}(\mathbf{x}_c)\end{bmatrix} \tag{8}$$

is chosen as a virtual output of (1). The feedback linearization is inferred from the first and second total time-derivative of (8), i.e.,

$$\dot{\tilde{\mathbf{y}}}=\begin{bmatrix}\mathrm{d}\lambda\mathbf{x}_v\\ \mathrm{d}\pi\mathbf{x}_v\end{bmatrix},\ \ddot{\tilde{\mathbf{y}}}=\underbrace{\begin{bmatrix}\dot{\mathrm{d}}\lambda\mathbf{x}_v+\mathrm{d}\lambda\mathbf{f}_v\\ \dot{\mathrm{d}}\pi\mathbf{x}_v+\mathrm{d}\pi\mathbf{f}_v\end{bmatrix}}_{\mathbf{b}(\mathbf{x})}+\underbrace{\begin{bmatrix}\mathrm{d}\lambda\mathbf{G}_v\\ \mathrm{d}\pi\mathbf{G}_v\end{bmatrix}}_{\mathbf{D}_u(\mathbf{x})}\mathbf{u}-\underbrace{\begin{bmatrix}\mathrm{d}\lambda\\ \mathrm{d}\pi\end{bmatrix}}_{\mathbf{D}_d(\mathbf{x})}\mathbf{d}. \tag{9}$$

Introducing the new input $\mathbf{v}^{\mathrm{T}}=\begin{bmatrix}v_{\parallel} & v_{\perp}\end{bmatrix}=\ddot{\tilde{\mathbf{y}}}$ and solving (9) for $\mathbf{u}$ yields the input-output feedback linearization, see, e.g., [12],

$$\mathbf{u}=\mathbf{D}_u^{-1}(\mathbf{x})\left(-\mathbf{b}(\mathbf{x})+\mathbf{D}_d(\mathbf{x})\mathbf{d}+\mathbf{v}\right)\big|_{\mathbf{x}=\mathbf{T}^{-1}(\boldsymbol{\eta},\boldsymbol{\xi})}. \tag{10}$$

Inserting the feedback transformation (10) with (7) into (1) results in linear system dynamics of the form

$$\dot{\xi}_1=\xi_2,\quad \dot{\xi}_2=v_{\perp},\quad \dot{\eta}_1=\eta_2,\quad \dot{\eta}_2=v_{\parallel}. \tag{11}$$

It is worth noting that the dynamics of the transformed system are linear with respect to the nonlinear path γ. Thus, the virtual input $v_{\perp}$ can effectively be used to stabilize the origin of the transverse $\boldsymbol{\xi}$-subsystem and $v_{\parallel}$ can be utilized to control the motion along the path. The tracking errors $e_{\eta}^p=\eta_1-\eta_1^p$ and $e_{\xi}^p=\xi_1-\xi_1^p$ are introduced with the sufficiently smooth path reference trajectories η_1^p and ξ_1^p along the path and transversal to the path, respectively. Eventually, the control laws

$$\begin{aligned}v_{\parallel}&=\ddot{\eta}_1^p-a_{\eta,2}\dot{e}_{\eta}^p-a_{\eta,1}e_{\eta}^p-a_{\eta,0}\int_0^t e_{\eta}^p\mathrm{d}\tau\\ v_{\perp}&=\ddot{\xi}_2^p-a_{\xi,2}\dot{e}_{\xi}^p-a_{\xi,1}e_{\xi}^p-a_{\xi,0}\int_0^t e_{\xi}^p\mathrm{d}\tau\end{aligned} \tag{12}$$

yield the linear, exponentially stable error dynamics

$$\begin{aligned}\left(e_{\eta}^p\right)^{(3)}+a_{\eta,2}\ddot{e}_{\eta}^p+a_{\eta,1}\dot{e}_{\eta}^p+a_{\eta,0}e_{\eta}^p=0\\ \left(e_{\xi}^p\right)^{(3)}+a_{\xi,2}\ddot{e}_{\xi}^p+a_{\xi,1}\dot{e}_{\xi}^p+a_{\xi,0}e_{\xi}^p=0\end{aligned}$$

that can be arbitrarily assigned by means of the constants $a_{l,k}>0$ for $l\in\{\eta,\xi\}$, $k=0,1,2$. An anti-windup strategy can be used to account for input constraints.

IV. COMPLIANCE CONTROL

Compliance control addresses a classical problem in robotics of simultaneously controlling the position and the interaction force with the environment. A well-known approach in literature, see, e.g., [8], is referred to as impedance control. The fundamental idea of the concept is to design a controller such that the system establishes a desired dynamic relationship between an external (projected) force

$$\bar{\mathbf{F}}_L=\begin{bmatrix}F_{\parallel}\\ F_{\perp}\end{bmatrix}=\begin{bmatrix}\left(\boldsymbol{\sigma}'(\theta)\right)^{\mathrm{T}}\mathbf{F}_L\\ \left(\boldsymbol{\kappa}(\theta)\right)^{\mathrm{T}}\mathbf{F}_L\end{bmatrix} \tag{13}$$

and the state errors $e_{\eta}^d=\eta_1-\eta_1^d$ and $e_{\xi}^d=\xi_1-\xi_1^d$ and their time derivatives. Herein, η_1^d and ξ_1^d denote the transversal and tangential reference trajectory, respectively. Typically, this relationship is specified in a linear form

$$\bar{\mathbf{F}}_L=\underbrace{\begin{bmatrix}m_{\parallel}&0\\ 0&m_{\perp}\end{bmatrix}}_{\mathbf{M}_d}\begin{bmatrix}\ddot{e}_{\eta}^d\\ \ddot{e}_{\xi}^d\end{bmatrix}+\underbrace{\begin{bmatrix}d_{\parallel}&0\\ 0&d_{\perp}\end{bmatrix}}_{\mathbf{D}_d}\begin{bmatrix}\dot{e}_{\eta}^d\\ \dot{e}_{\xi}^d\end{bmatrix}+\underbrace{\begin{bmatrix}k_{\parallel}&0\\ 0&k_{\perp}\end{bmatrix}}_{\mathbf{K}_d}\begin{bmatrix}e_{\eta}^d\\ e_{\xi}^d\end{bmatrix}, \tag{14}$$

where the positive definite matrices $\mathbf{M}^d$, $\mathbf{D}^d$, and $\mathbf{K}^d$ represent the desired inertia, damping, and stiffness, respectively. If the matrices are diagonal, the compliances in tangential and transversal direction are decoupled. Thus, $m_j>0, d_j>0$ and $k_j>0$ for $j\in\{\parallel,\perp\}$ are the inertia, damping, and stiffness in tangential and transversal direction.

Post-print version of the article: S. Flixeder, T. Glück, M. Böck, and A. Kugi, "Combined path following and compliance control with application to a biaxial gantry robot", in *Proceedings of the IEEE Conference on Control Applications (CCA)*, Antibes, France, Oct. 2014, pp. 796–801. DOI: 10.1109/CCA.2014.6981438

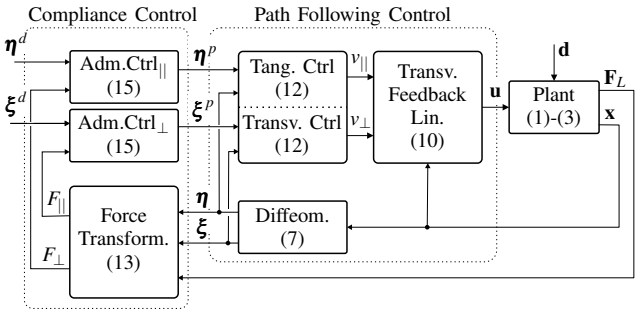

Fig. 3. Path following and compliance control scheme.

A. Admittance Control

In order to achieve a desired impedance behavior, the so-called admittance control [10], often denoted as *position-based impedance control* [13] or *inner/outer impedance control* [14], approach is utilized. The compliant behavior is realized by tracking the trajectory of a desired impedance model using the transverse and tangential feedback linearization in the inner loop and the admittance control in the outer loop, see Fig. 3. Assuming perfect tracking performance of the inner position controller, one may replace the actual transverse and tangential state η_1 and ξ_1 in (14) with the path reference trajectories η_1^p and ξ_1^p. Introducing the errors $e_\eta^{pd} = \eta_1^p - \eta_1^d$ and $e_\xi^{pd} = \xi_1^p - \xi_1^d$, the admittance control laws read as

$$\begin{aligned}
\ddot{\eta}_1^p &= \ddot{\eta}_1^d + \frac{F_\parallel}{m_\parallel} - \frac{d_\parallel}{m_\parallel}\dot{e}_\eta^{pd} - \frac{k_\parallel}{m_\parallel}e_\eta^{pd}, \qquad \dot{\eta}_1^p = \int_0^t \ddot{\eta}_1^p \mathrm{d}\tau \\
\ddot{\xi}_1^p &= \ddot{\xi}_1^d + \frac{F_\perp}{m_\perp} - \frac{d_\perp}{m_\perp}\dot{e}_\xi^{pd} - \frac{k_\perp}{m_\perp}e_\xi^{pd}, \qquad \dot{\xi}_1^p = \int_0^t \ddot{\xi}_1^p \mathrm{d}\tau \\
\eta_1^p &= \int_0^t \dot{\eta}_1^p \mathrm{d}\tau, \qquad \xi_1^p = \int_0^t \dot{\xi}_1^p \mathrm{d}\tau,
\end{aligned} \tag{15}$$

yielding the exponentially stable closed-loop dynamics in tangential and transversal direction of the form

$$\begin{aligned}
F_\parallel &= m_\parallel \ddot{e}_\eta^{pd} + d_\parallel \dot{e}_\eta^{pd} + k_\parallel e_\eta^{pd} \\
F_\perp &= m_\perp \ddot{e}_\xi^{pd} + d_\perp \dot{e}_\xi^{pd} + k_\perp e_\xi^{pd}.
\end{aligned}$$

Consequently, the compliance in transversal and tangential direction of the path are now decoupled, can be chosen independently, and do not depend on the position along the curve. Moreover, as the transformed states $(\boldsymbol{\eta}, \boldsymbol{\xi})$ show the property $\|\mathrm{d}\eta_1\| = \|\mathrm{d}\xi_1\| = 1$ for $\mathbf{y} \in \gamma$, no adjustment of the desired impedance parameters is required when choosing different paths.

In order to account for the velocity and the acceleration limits of the physical system, conditional execution and integration is performed to implement (15). Since system model uncertainties are compensated by the inner position control loop, this strategy provides high impedance tracking accuracy in the non-contact case and greatly facilitates the implementation on standard industrial manipulators with high and/or unknown friction forces [9].

TABLE I
2-DOF GANTRY ROBOT COMPONENTS

component	manufacturer	type
y-axis ball screw	FESTO	*EGC-80-BS-KF-1200*
z-axis ball screw	FESTO	*EGC-70-BS-KF-800*
servo motor	FESTO	*AS-55-M*
force sensor	ME-MESSSYSTEME	*K3D40*

Note that the interaction with environment is not systematically considered yet and especially in case of stiff environments the perfect tracking assumption may no longer hold and impedance errors are likely to occur. These classical robustness and stability issues of the admittance approach are intensively studied in literature, see, e.g., [9], [15].

B. Force Tracking Control

Many applications do not ask for a desired impedance behavior, but rather demand to maintain a desired interaction force with an environment while following a reference trajectory in the output space. Therefore, [16] suggests a control law that is inferred from (14) by subtracting the desired force $\bar{\mathbf{F}}_L^d$ from the measured load force $\bar{\mathbf{F}}_L$ and setting the stiffness $\mathbf{K}_d$ to zero. Thus, the force tracking control law is equivalent to (14), except that $F_\parallel$ and $F_\perp$ are replaced by $F_\parallel - F_\parallel^d$ and $F_\perp - F_\perp^d$ and $k_\parallel = k_\perp = 0$. Under the assumption that the environment behaves like a nonlinear spring

$$F_\parallel = -f_\parallel\left(e_\eta^d\right), \quad F_\perp = -f_\perp\left(e_\xi^d\right),$$

where $e_\eta^d f_\parallel\left(e_\eta^d\right) > 0$ and $e_\xi^d f_\perp\left(e_\xi^d\right) > 0$, and perfect tracking performance of the inner position controller, the equilibrium of the closed-loop dynamics

$$\begin{aligned}
-F_\parallel^d &= m_\parallel \ddot{e}_\eta^{pd} + d_\parallel \dot{e}_\eta^{pd} + f_\parallel\left(e_\eta^{pd}\right) \\
-F_\perp^d &= m_\perp \ddot{e}_\xi^{pd} + d_\perp \dot{e}_\xi^{pd} + f_\perp\left(e_\xi^{pd}\right)
\end{aligned}$$

is asymptotically stable. Thus, the desired forces $F_\parallel^d$ and $F_\perp^d$ serve as driving forces to exert specific forces on the environment and in steady state condition, $F_\parallel = F_\parallel^d$ and $F_\perp = F_\perp^d$ holds.

V. EXPERIMENTAL RESULTS

Measurement results of the 2-DOF gantry robot are shown in this section. The servo motors as well as the ball screw drives are from FESTO. The end effector position and velocity are calculated from the measurements of the integrated motor encoders. A triaxial force sensor form ME-MESSSYSTEME is used to measure the external forces acting on the end effector. Details on the components are listed in Table I. The model parameters are either extracted from data-sheets or measurements and are summarized in Table II. The presented control algorithms are implemented and executed using a real-time system *DS1006* from DSPACE at

Post-print version of the article: S. Flixeder, T. Glück, M. Böck, and A. Kugi, "Combined path following and compliance control with application to a biaxial gantry robot", in *Proceedings of the IEEE Conference on Control Applications (CCA)*, Antibes, France, Oct. 2014, pp. 796–801. DOI: 10.1109/CCA.2014.6981438

TABLE II

2-DOF GANTRY ROBOT PARAMETERS

i-axis	$m_{t,i}$	$m_{J,i}$	$F_{c,i}$	$c_{v,i}$
y-axis	7.61 kg	29.26 kg	65.42 N	175.93 N s m^{-1}
z-axis	4.41 kg	16.79 kg	37.69 N	62.83 N s m^{-1}

TABLE III

DESIRED IMPEDANCE PARAMETERS

j-direction	m_j	ζ_j	k_j
$\perp$-direction	2.0 kg	0.3	200 N m^{-1}
$\parallel$-direction	0.5 kg	0.6	10 N m^{-1}

a sampling time of 1 ms. For illustration purpose, the desired path is chosen as an ellipse, which can be written as

$$\hat{\boldsymbol{\sigma}}(\hat{\theta}) = \begin{bmatrix} a\cos(\hat{\theta}) + s_{y,o} \\ b\sin(\hat{\theta}) + s_{z,o} \end{bmatrix}, \tag{16}$$

with the length of the major and minor axes $a = 0.3$ m and $b = 0.15$ m, and its center coordinates $s_{y,0} = 0.5$ m, $s_{z,0} = 0.5$ m with respect to the reference frame. Note that (16) is not in unit speed parametrization. Additionally, we want to emphasize that more complicated paths such as splines can be implemented with the same approach. In the following experiments, the controller parameters $a_{l,k} > 0$ for $l \in \{\eta, \xi\}$, $k = 0, 1, 2$ were chosen such that the eigenvalues of the closed-loop error dynamics are $p_{\perp,k} = -40\,\text{s}^{-1}$ and $p_{\parallel,k} = -20\,\text{s}^{-1}$ for $k = 0, 1, 2$. The desired impedance parameters in tangential and transversal direction were selected according to Table III, where ζ_j represents the damping ratio and the desired damping follows as $d_j = 2\zeta_j\sqrt{m_j/k_j}$, for $j \in \{\parallel, \perp\}$.

A. Experiment A - Path Following Control

In a first experiment, only the path following concept presented in Section III is investigated. Thus, solely the performance of the inner position control loop is examined. Fig. 4 shows the position of the end effector $\mathbf{x}_c$ of the gantry robot in the output space and the corresponding transformed states ξ_1 and η_1. Starting from an initial position $\mathbf{x}_c(0)$, tracking errors in transversal and tangential direction are quickly regulated to zero. Subsequently, set-point changes in the transversal and tangential direction are performed. Despite existing model inaccuracies, in particular in terms of friction, the tracking performance is clearly satisfactory.

B. Experiment B - Path Following and Compliance Control

The second experiment combines the path following approach of Section III and the compliance control strategy presented in Section IV. The path reference trajectories η_1^p and ξ_1^p of the inner path following controller are generated by the admittance controllers in the outer loop, see Fig. 3. The inner control loop tracks these generated path reference trajectories and realizes the impedance behavior according to (14) with the parameters listed in Table III. Starting from an initial position $\mathbf{x}_c(0)$, a position change along the path by means of η_1^d is accomplished, see Fig. 5. Accordingly, the

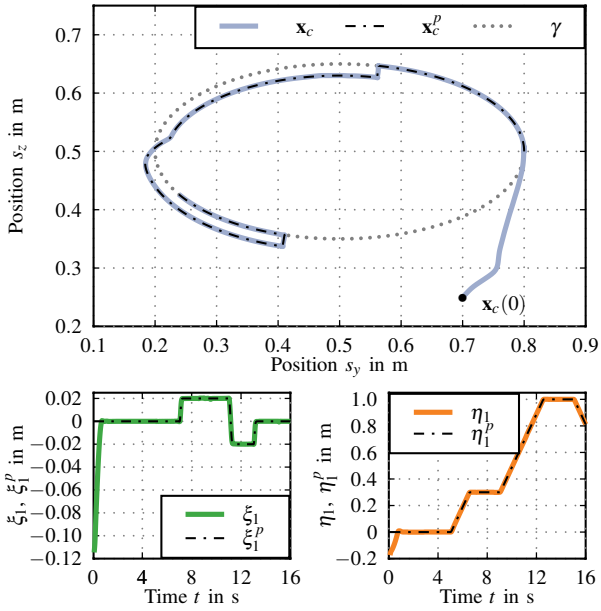

Fig. 4. Experiment A: Following an elliptic path γ in the output space according to the path reference trajectories η_1^p and ξ_1^p.

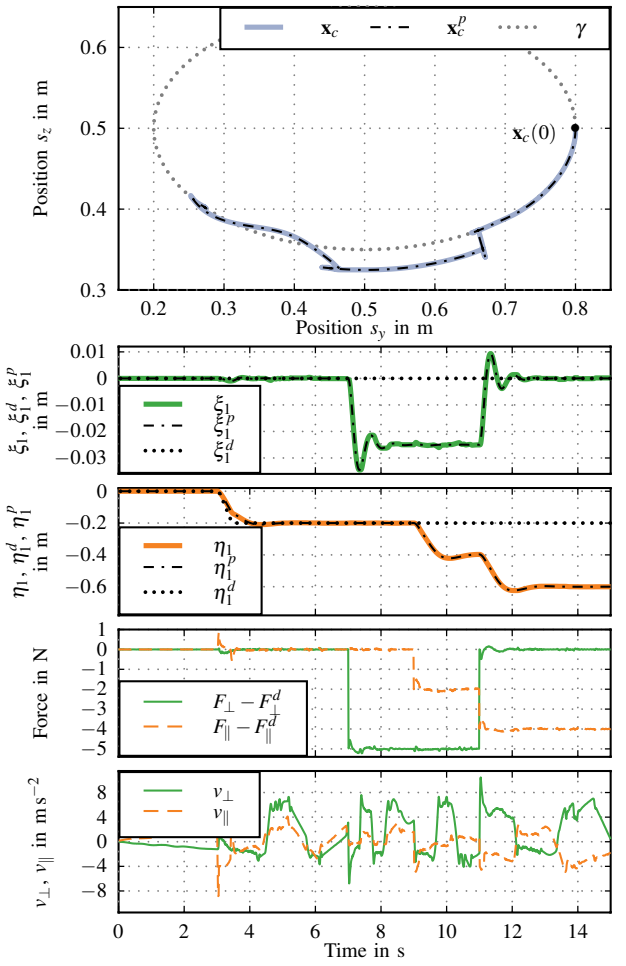

Fig. 5. Experiment B: Combined path following and compliance control for an elliptic path γ.

Post-print version of the article: S. Flixeder, T. Glück, M. Böck, and A. Kugi, "Combined path following and compliance control with application to a biaxial gantry robot", in *Proceedings of the IEEE Conference on Control Applications (CCA)*, Antibes, France, Oct. 2014, pp. 796–801. DOI: 10.1109/CCA.2014.6981438

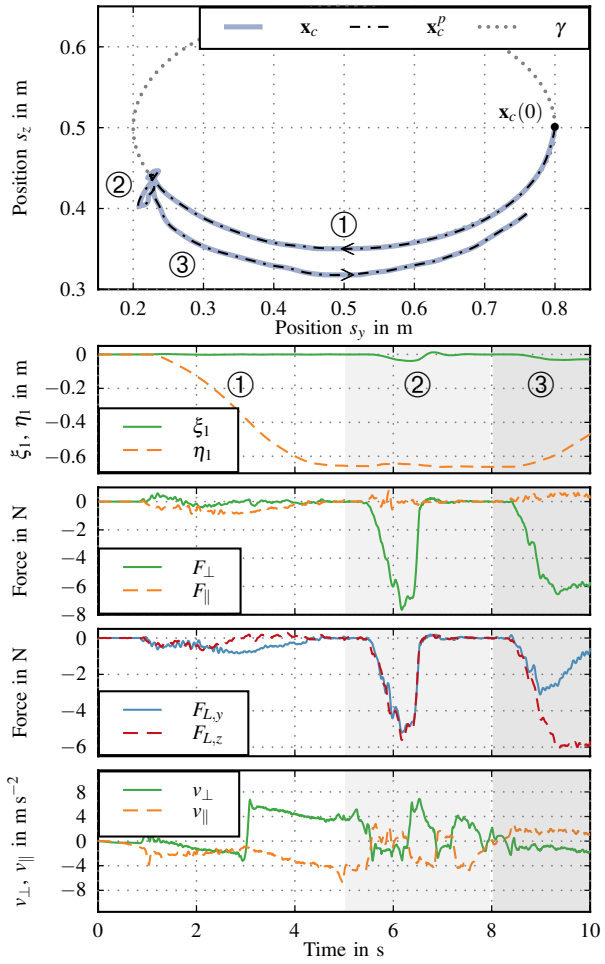

Fig. 6. Experiment C: Combined path following and compliance control for an elliptic path γ as forces are applied by a human operator.

system responds with the desired impedance behavior in path direction. Next, a desired force $F_\perp^d = 5\,\mathrm{N}$ is subtracted from the (projected) measured force $F_\perp$ in transversal direction. Thus, the gantry robot reacts like an equivalent desired damped system in the path normal direction. Subsequently, a desired force $F_\parallel^d = 2\,\mathrm{N}$ is applied in tangential direction and causes the output to move in path direction. However, ξ_1 remains at its set point, as $F_\perp^d$ is constantly applied. At last, the forces $F_\perp^d$ and $F_\parallel^d$ are changed simultaneously, whereupon the system responds accordingly. The peaks in the projected force signals result from the uncompensated inertial force of the end effector acting on the force sensor in case of dynamic position changes. The abrupt changes of the transversal and tangential control inputs $v_\perp$ and $v_\parallel$ are due to the not perfectly compensated Coulomb friction.

C. Experiment C - Path Following and Force Control

In the last experiment, presented in Fig. 6, the stiffness $k_\parallel$ of the tangential subsystem is set to zero and an external force $\mathbf{F}_L$ is manually applied. The applied force in transversal direction is comparatively low at the first part of the experiment, hence only movements along the path are induced. In the second part, the human operator increases the force in normal direction and therefore causes desired deviations normal to the path. At last, forces are applied in transversal and tangential direction resulting in a transversal deviation and a guided motion along the path.

VI. CONCLUSIONS

This paper presents the design of a combined path following and compliance controller exemplarily applied to a biaxial gantry robot. Although the proposed controller is designed for a comparatively simple robotic manipulator, we emphasize that the proposed concept is applicable to any other industrial robot satisfying the assumptions of [7]. This approach may also greatly facilitate human machine interaction, i.e., as the workspace of the robot can be limited to a desired path, where the human operator controls the motion along the path.

REFERENCES

[1] J. Pandremenos, C. Doukas, P. Stavropoulos, and G. Chryssolouris, "Machining with robots: a critical review," in *Proc. 7th International Conference on Digital EnterpriseTechnology*, Athens, Greece, Sep. 2011, pp. 614–621.

[2] G. Zeng and A. Hemami, "An overview of robot force control," *Robotica*, vol. 15, no. 5, pp. 473–482, 1997.

[3] T. M. Stepien, L. M. Sweet, M. C. Good, and M. Tomizuka, "Control of tool/workpiece contact force with application to robotic deburring," *IEEE J. Robot. Autom.*, vol. RA-3, no. 1, pp. 7–18, 1987.

[4] Z. Pan and H. Zhang, "Robotic machining from programming to process control," in *Proc. 7th World Congresson Intelligent Control and Automation*, Chongqing, China, Jun. 2008, pp. 553–558.

[5] C. Nielsen, C. Fulford, and M. Maggiore, "Path following using transverse feedback linearization: Application to a maglev positioning system," in *Proc. American Control Conference*, St. Louis, MO, USA, Jun. 2009, pp. 3045–3050.

[6] L. Consolini, M. Maggiore, C. Nielsen, and M. Tosques, "Path following for the PVTOL aircraft," *Automatica*, vol. 46, no. 8, pp. 1284–1296, 2010.

[7] A. Hladio, C. Nielsen, and D. Wang, "Path following controller design for a class of mechanical systems," in *Proc. 18th IFAC World Congress*, Milano, Italy, Aug./Sep. 2011, pp. 10 331–10 336.

[8] N. Hogan, "Impedance control: An approach to manipulation: Part ii – implementation," *Journal of Dynamic Systems, Measurement, and Control*, vol. 107, no. 1, pp. 8–16, 1985.

[9] D. Šurdilović, "Contact stability issues in position based impedance control: Theory and experiments," in *Proc. IEEE InternationalConference on Robotics and Automation*, vol. 2, Minneapolis, MN, USA, Apr. 1996, pp. 1675–1680.

[10] C. Ott, A. Kugi, and G. Hirzinger, "On the passivity-based impedance control of flexible joint robots," *IEEE Trans. Robot.*, vol. 24, no. 2, pp. 416–429, 2008.

[11] A. Hladio, C. Nielsen, and D. Wang, "Path following for a class of mechanical systems," *IEEE Trans. Control Syst. Technol.*, vol. 21, no. 6, pp. 2380–2390, 2013.

[12] A. Isidori, *Nonlinear Control Systems*, 3rd ed. London: Springer, 1995.

[13] G. J. Liu and A. A. Goldenberg, "Robust hybrid impedance control of robot manipulators," in *Proc. IEEE International Conference on Robotics and Automation*, vol. 1, Sacramento, CA, USA, Apr. 1991, pp. 287–292.

[14] D. A. Lawrence, "Impedance control stability properties in common implementations," in *Proc. IEEE InternationalConference on Robotics and Automation*, vol. 2, Philadelphia, PA, USA, Apr. 1988, pp. 1185–1190.

[15] T. Valency and M. Zacksenhouse, "Accuracy/robustness dilemma in impedance control," *Journal of Dynamic Systems, Measurement, and Control*, vol. 125, no. 3, pp. 310–319, 2003.

[16] S. Jung, T. C. Hsia, and R. G. Bonitz, "Force tracking impedance control of robot manipulators under unknown environment," *IEEE Trans. Control Syst. Technol.*, vol. 12, no. 3, pp. 474–483, 2004.

Post-print version of the article: S. Flixeder, T. Glück, M. Böck, and A. Kugi, "Combined path following and compliance control with application to a biaxial gantry robot", in *Proceedings of the IEEE Conference on Control Applications (CCA)*, Antibes, France, Oct. 2014, pp. 796–801. DOI: 10.1109/CCA.2014.6981438